Monthly Notices
of the
ROYAL ASTRONOMICAL SOCIETY

Mon. Not. R. Astron. Soc. **423,** 1293–1299 (2012) doi:10.1111/j.1365-2966.2012.20951.x

Intensity and polarization of the atmospheric emission at millimetric wavelengths at Dome Concordia

E. S. Battistelli,[1⋆] G. Amico,[1] A. Baù,[2] L. Bergé,[3] É. Bréelle,[4] R. Charlassier,[4] S. Collin,[3] A. Cruciani,[1] P. de Bernardis,[1] C. Dufour,[4] L. Dumoulin,[3] M. Gervasi,[2] M. Giard,[5] C. Giordano,[1,6] Y. Giraud-Héraud,[4] L. Guglielmi,[4] J.-C. Hamilton,[4] J. Landé,[5] B. Maffei,[7] M. Maiello,[1,8] S. Marnieros,[3] S. Masi,[1] A. Passerini,[2] F. Piacentini,[1] M. Piat,[4] L. Piccirillo,[7] G. Pisano,[7] G. Polenta,[1,9,10] C. Rosset,[4] M. Salatino,[1] A. Schillaci,[1] R. Sordini,[1,11] S. Spinelli,[2,12] A. Tartari[2,4] and M. Zannoni[2]

[1]*Dipartimento di Fisica, 'Sapienza' Università di Roma, Piazzale Aldo Moro, 5, 00185, Rome, Italy*
[2]*Dipartimento di Fisica 'G. Occhialini', Università degli Studi di Milano-Bicocca, Piazza della Scienza, 3, 20126, Milan, Italy*
[3]*Centre de Spectroscopie Nucléaire et de Spectroscopie de Masse, UMR8609 IN2P3-CNRS, Université Paris Sud, bât 108, 91405, Orsay Campus, France*
[4]*APC, Université Paris, Diderot-Paris 7, CNRS/IN2P3, CEA, Observatoire de Paris, 10, rue A. Domon and L. Duquet, Paris, France*
[5]*Centre d'Étude Spatiale des Rayonnements, CNRS/Université de Toulouse, 9 Avenue du colonel Roche, BP 44346, 31028, Toulouse Cedex 04, France*
[6]*Fondazione Bruno Kessler, Via S. Croce 77, 38122, Trento, Italy*
[7]*JBCA School of Physics and Astronomy, The University of Manchester, Alan Turing Building, Oxford Road, Manchester M13 9PL*
[8]*Università degli Studi di Siena, Via Banchi di Sotto 55, 53100, Siena, Italy*
[9]*ASI Science Data Centre, c/o ESRIN, via G. Galilei, 00044, Frascati, Italy*
[10]*INAF – Osservatorio Astronomico di Roma, via di Frascati 33, 00040 Monte Porzio Catone, Italy*
[11]*Dipartimento di Scienze Applicate, Università degli Studi di Napoli 'Parthenope', Centro Direzionale di Napoli, Isola C4, 80143, Naples, Italy*
[12]*Media Lario Technologies S.r.l., Località Pascolo, 23842, Bosisio Parini (LC), Italy*

Accepted 2012 March 18. Received 2012 March 16; in original form 2011 December 23

ABSTRACT

Atmospheric emission is a dominant source of disturbance in ground-based astronomy at millimetric wavelengths. The Antarctic plateau is recognized as an ideal site for millimetric and submillimetric observations, and the French/Italian base of Dome Concordia (Dome C) is among the best sites on Earth for these observations. In this paper, we present measurements at Dome C of the atmospheric emission in intensity and polarization at a 2-mm wavelength. This is one of the best observational frequencies for cosmic microwave background (CMB) observations when considering cosmic signal intensity, atmospheric transmission, detector sensitivity and foreground removal. Using the B-mode radiation interferometer (BRAIN)-pathfinder experiment, we have performed measurements of the atmospheric emission at 150 GHz. Careful characterization of the airmass synchronous emission has been performed, acquiring more than 380 elevation scans (i.e. 'skydip') during the third BRAIN-pathfinder summer campaign in 2009 December/2010 January. The extremely high transparency of the Antarctic atmosphere over Dome C is proven by the very low measured optical depth, $\langle \tau_{\rm I} \rangle = 0.050 \pm 0.003 \pm 0.011$, where the first error is statistical and the second is the systematic error. Mid-term stability, over the summer campaign, of the atmosphere emission has also been studied. Adapting the radiative transfer atmosphere emission model *am* to the particular conditions found at Dome C, we also infer the level of the precipitable water vapor (PWV) content of the atmosphere, which is notoriously the main source of disturbance in millimetric astronomy ($\langle PWV \rangle = 0.77 \pm 0.06 \pm^{0.15}_{0.12}$ mm). Upper limits on the airmass correlated polarized signal are also placed for the first time. The degree of circular polarization of atmospheric emission is found to be lower than 0.2 per cent [95 per cent confidence level (CL)], while the

⋆E-mail: elia.battistelli@roma1.infn.it

degree of linear polarization is found to be lower than 0.1 per cent (95 per cent CL). These limits include signal-correlated instrumental spurious polarization.

Key words: atmospheric effects – instrumentation: polarimeters – site testing – cosmic background radiation.

1 INTRODUCTION

The study of the cosmic microwave background (CMB) polarization and the measurement of polarized emission from interstellar dust are fast growing fields in millimetric astronomy. In particular, a curl component (B-modes) of the CMB polarization, from the predicted inflationary expansion of the Universe earlier in time, might be present. The theorized signal depends on the energy of the inflationary field, as measured by the tensor-to-scalar ratio r. It is so low that exceptional sensitivity and control of systematic effects are necessary to attempt these types of observations.

Atmospheric emission is one of the dominant sources of disturbance for ground-based CMB experiments, and for millimetric and submillimetric astronomy in general. In addition to continuum emission at the frequencies in which we are interested, there are also the roto-vibrational emission lines of O_2 (at around 60 and 119 GHz) and H_2O (at 22 and 183 GHz). Dry and high-altitude observation sites are chosen to mitigate the problem. The French/Italian scientific base of Dome Concordia (Dome C) on the Antarctic plateau ($75^\circ 06'$ south, $123^\circ 24'$ east, at 3233 m above sea level[1]) is one of the best observational sites on Earth for millimetric observations. Site testing at Dome C has proven its observational quality at different wavelengths (e.g. Calisse et al. 2004; Lawrence et al. 2004; Aristidi et al. 2009; Gredel 2010; Tremblin et al. 2011), although only preliminary measurements were performed at millimetre wavelengths (Valenziano & dall'Oglio 1999). In terms of cosmic signal intensity, atmospheric transmission, detector sensitivity and foreground removal, 150 GHz is among the best observational frequencies for ground-based CMB experiments.

The B-mode radiation interferometer (BRAIN)-pathfinder experiment (Masi et al. 2005; Polenta et al. 2007) has undergone its third Antarctic campaign from the French/Italian scientific base of Dome C. The first two campaigns were dedicated to instrument fielding, while the 2009–2010 austral summer campaign was dedicated to continuous observations of the atmospheric emission and to site testing.

This paper is structured as follows. In Section 2, we introduce the BRAIN-pathfinder instrument, and in Section 3 we describe the observations. In Section 4, we present the data and the analysis, and in Section 5 we give the results in terms of intensity and polarization.

2 BRAIN-PATHFINDER: THE INSTRUMENT

The BRAIN-pathfinder was designed as a prototype instrument for a challenging project for a bolometric interferometer. The BRAIN collaboration has been combined with the millimetre-wave bolometric interferometer (MBI) collaboration (Tucker et al. 2008) to form the QUBIC collaboration. The BRAIN-pathfinder was devoted to site and logistics testing for the QUBIC experiment (Battistelli et al., QUBIC collaboration 2011), which we aim to install at Dome C in 2013. The BRAIN-pathfinder instrument is described in detail elsewhere (Masi et al. 2005; Polenta et al. 2007; Masi et al., in preparation). Nevertheless, here we give a brief description of the instrumental set-up for completeness.

The BRAIN-pathfinder comprises a two-channel bolometric receiver coupled to two off-axis (40- and 60-cm diameter) parabolic mirrors, which can be tilted around the optical axis. The whole instrument is mounted on an azimuth plane, making the instrument an Alt-Az double telescope. The first in its kind, our bolometric receiver is cooled by a dry-cryostat with a Sumitomo[2] Pulse Tube cryocooler, which allows us to keep an intermediate stage at 30 K and a main plate at 3 K. Quasi-optical filters, JFET boards and shields are kept at 30 K with JFET amplifiers attached to their PCB through weak thermal connections in their fibre glass supports. Further filters, radiation-collecting horns and further shields are kept at 3 K with an ^{3}He–^{4}He refrigerator,[3] which keeps the bolometers at 310 mK during observations.

One of the two channels (channel 1) measures the anisotropy of the emission of the sky, while the second (channel 2) sees the sky through an ambient-temperature, rotating sapphire quarter-wave plate (QWP) and a steady wire grid polarizer. The presence of the rotating QWP makes this second detector inherently sensitive to linear and circular polarization. In an ideal case, the power hitting channel 2 is thus (Polenta et al. 2007)

$$W = \frac{1}{2}\left[I_{\rm in} + Q_{\rm in}\frac{1+\cos(4\omega t)}{2} + U_{\rm in}\frac{\sin(4\omega t)}{2} + V_{\rm in}\sin(2\omega t)\right]. \quad (1)$$

Here, $I_{\rm in}$, $Q_{\rm in}$, $U_{\rm in}$ and $V_{\rm in}$ are the Stokes parameters of the incoming radiation and ω is the mechanical angular speed of the QWP. From equation (1), it is clear that an incoming polarized radiation is modulated by the rotating QWP at frequencies twice or four times the mechanical frequency, depending on whether the polarization is circular or linear.

We use the control and readout electronics, as well as the control software, originally developed for the *Planck* high-frequency instrument (Lamarre et al. 2010) and for its ground-based calibrations. Its angular resolution on the sky is 1°. A double back-to-back horn and the quasi-optical filters set the average observational frequency at 150 GHz, with a 36-GHz FWHM bandwidth. Detailed measurements of the bandpass have been performed, combining data obtained with a high-throughput Fourier transform spectrometer (Schillaci 2010) and a vector network analyser[4] in order to characterize the transmission curve, especially on the low-frequency end of the bandpass, where the molecular oxygen-line emission becomes brighter.

3 OBSERVATIONS

Observations were taken during the 2009–2010 austral summer Antarctic campaign. In contrast to a CMB experiment, for which

[1] http://www.concordiabase.eu/

[2] http://www.shicryogenics.com/

[3] http://www.chasecryogenics.com/

[4] http://www.home.agilent.com/agilent/home.jspx

one should choose an observational strategy aimed at minimizing the atmospheric effects (e.g. Castro et al. 2009; Chiang et al. 2010), we have chosen an observational strategy able to highlight the atmospheric contribution. Here, we present a full characterization of the airmass dependence of the atmospheric intensity and polarized emission, obtained by performing elevation scans (i.e. skydips) by leaving the azimuth constant and by scanning the elevation from the zenith to 35° above the horizon.

Elevation scans were performed in a so-called 'fast scan' mode by acquiring the sky signal while the telescope continuously samples different elevation angles. The scan speed has been chosen to be as high as possible, in order to mitigate the $1/f$ noise present in the data, arising both from detector instability and (mainly) from the slow variation of the atmospheric emission. At the same time, we set the scan speed to be able to acquire multiple QWP rotations in one single telescope beam. We tested different QWP and scan speeds, trading off instrumental constraints and observational needs. We set the QWP rotational frequency at 1.56 Hz (corresponding to 3.13 and 6.26 Hz, respectively, for circular and linear polarization modulation frequencies) for approximately half of the measurements, and at 2.09 Hz (corresponding to 4.17 and 8.35 Hz, respectively, for circular and linear polarization modulation frequencies) for the rest of the time. A scan speed of $1^\circ\ s^{-1}$ thus allows at least three or six polarized modulation periods per telescope beam. With these settings, a full scan completes in less than a minute, a short enough time to mitigate slow signal variation arising from atmospheric emission.

In order to reduce the field-of-view vignetting, to overcome detector and readout non-linearity, and to optimize the detector dynamics, we have chosen not to use a warm reference load for skydip measurements. This forces us to make some assumptions if we want to carry out absolute calibration of the data (see Section 4). However, it allows us to directly analyse the polarization data relative to the intensity emission, with no need for any reference signal.

We have collected 383 skydips. About 12 per cent of the skydips were discarded because of corrupted data or because of large atmospheric fluctuations. About 76 per cent of the analysed skydips were acquired by changing the elevation from the zenith to 35° above the horizon (long skydip). The remaining 24 per cent were limited to 60° above the horizon (short skydip), in order to keep the Sun always at an angle larger than 30° from the field of view. Most of the reported results have been extracted from the analysis of the long skydips, although the short skydips have been useful for cross-checks.

4 DATA REDUCTION AND ANALYSIS

The skydip technique (Dicke et al. 1946) is a well-investigated method to study the atmospheric emission (e.g. Dragovan et al. 1990; Archibald et al. 2002). During a skydip, we expect the acquired signal to respond to the airmass as follows:

$$S = off + C\,T_0[1 - \exp(-x\tau_1)]. \quad (2)$$

Here, S is the acquired signal in ADC units, *off* is an instrumental offset in ADC units, C is the calibration factor in ADC/K units, T_0 (in K) is the equivalent temperature of the atmosphere, τ_1 is the sky opacity and $x = \sec(z)$ is the airmass with the zenithal angle $z = 90^\circ -$ elevation.

One of the features in our data is the presence in the time stream of a periodic signal at a frequency of around 1 Hz as a result of the pulses of the Pulse Tube cryocooler. In fact, the experimental effort spent on reducing the system vibration has drastically reduced but not completely eliminated the effect of the pulses on the high impedence bolometers, which are intrinsically microphonic. This does not affect the high signal-to-noise skydip measurements we are analysing in this paper; nevertheless, we have decided to filter out from our data this well-defined imprint, in order to avoid biases in the skydip fits. We have performed several tests, both in time and in Fourier space, and we finally decided to use a multiple notch filter to remove the main pulse frequency and its harmonics. Fig. 1 shows the filtered and unfiltered signals (and their Fourier transforms), in engineering units, acquired during one skydip.

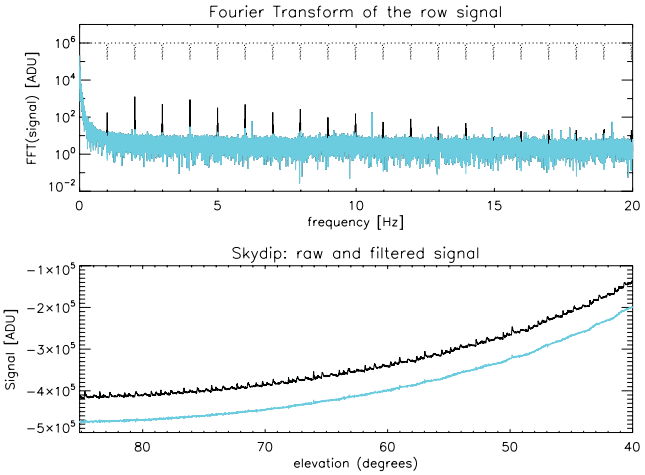

Figure 1. Data acquired during one skydip. The upper plot shows the Fourier transform of the raw data (black, solid), the used multiple notch filter (black, dotted) and the filtered data (cyan, solid, overplotted on the data). The lower plot shows a raw skydip (black) and a filtered skydip (cyan) offset by 60 000 analogue to digital units (ADU).

While for channel 1 we have only (notch-) filtered out the pulse tube 1-Hz signal, in order to retrieve signal intensity information from channel 2 we have to account for the presence of the rotating QWP in front of it. Thus, we have applied a low-pass filter, with a cut-off frequency at 1 Hz, to remove any higher frequency signal resulting from the rotating QWP, which could modulate the linear and circular polarized signal. Dedicated bandpass filters have then been applied to retrieve polarization information (see Section 5.3 for details).

We have performed a likelihood analysis and χ^2 minimization to optimize secant-law fits on each of the acquired skydips. We have verified the linearity of the dependence of the signal as a function of the airmass. This is verified only in the case of high transparency of the atmosphere:

$$S = P_1 + P_2\exp(-P_0x) \simeq P_1 + P_2 - P_2P_0x = A^{\rm I} - B^{\rm I}x. \quad (3)$$

Here, $A^{\rm I} = P_1 + P_2$ and $B^{\rm I} = P_2P_0$ are the fitted parameters.

Comparing equations (2) and (3), we determine the sky opacity,

$$\tau_1 = -B^{\rm I}/(C\,T_0), \quad (4)$$

where the calibration factor C has been determined by using laboratory absolute reference loads cooled at liquid nitrogen temperature (i.e. 77 K), by careful measurements of the bolometer efficiency, as well as the daily electrical responsivity measurements performed during observations through the measurements of the detector I–V curve. The temperature T_0 was determined by integrating the temperature, pressure and humidity profiles obtained by daily measurements with atmospheric radio-sound balloons flying up to an altitude of 24 000 m, collecting data with $\Delta h \sim 10$ m altitude

sampling.[5] In particular, combined with continuous ground-temperature measurements at the time of the skydip, and after integration of the atmospheric emission contribution over the altitude for each of our scans, these data allowed us to recover T_0 using radiative transfer.

Our model for atmosphere emission is made by two different parts; in order to reconstruct the circularly polarized O_2 signals, we use the model described in Spinelli et al. (2011). This model can be used to estimate also Stokes parameters I, Q and U. In order to deal with a complete dry-air model, together with a water vapour column, we used the *am* model (Paine et al. 2011). The *am* model uses updated spectroscopic parameters and it is readily available, very well supported and documented. We have made day-by-day estimates of the atmospheric emission using radio sounds, properly resampled to build *am* configuration files. The resulting brightness temperature is then averaged over the frequency bandpass of the BRAIN-pathfinder channels, after accurate laboratory bandpass reconstruction, to obtain the power delivered to our detectors. We find a linear scaling relation between the precipitable water vapour (PWV), or the integrated optical depth τ, and the brightness temperature T_b in our bandpass, that is

$$T_b = Q + M\,PWV. \quad (5)$$

Here, $M_{ch1} = (6.6 \pm 0.3)$ K mm^{-1}, $M_{ch2} = (5.4 \pm 0.3)$ K mm^{-1} and $Q = (4.2 \pm 0.2)$ K, with PWV expressed in mm. Not surprisingly, the two M coefficients are different, because our bandpasses are strongly suppressed towards the 118-GHz O_2 line, while their high-frequency wings pick up – with small (but not negligible) and different efficiency – a residual signal from the 183-GHz H_2O line. The intercept Q is sensitive to the dry-air component, mainly to O_2, whose tail is observed with the same efficiency by our detectors.

In order to account for polarized emission, it is necessary to consider the magnetic field direction and intensity. We have estimated these for the austral summer 2009/2010, at Dome C, using the International Geomagnetic Reference Field (IGRF) model. The day-by-day variation in atmospheric conditions produces a small uncertainty on the oxygen polarized and unpolarized brightness temperature computed through their model (seasonal variations and magnetic storms are definitely more relevant). In particular, in the specific case of the BRAIN campaign, the absolute uncertainty on O_2 modelled signals is of the order of a few μK and a few mK, respectively, for the V and I maps. Both these uncertainties are negligible with respect to the uncertainty associated with H_2O emission estimates, which is of the order of some tens of mK. This last uncertainty is driven mainly by the day-by-day scatter of atmospheric parameters.

We found the uncertainty derived from the fits to be negligible with respect to the estimated uncertainty derived from the calibration procedure. This can be as high as 23 per cent and it should be treated as a systematic error. It dominates over all other uncertainties. Calibration uncertainties proportionally propagate to the opacity determination, while we have produced Monte Carlo simulations in order to estimate PWV uncertainties.

Fig. 2 shows the best-fitting curves obtained over the calibrated skydips collected during the campaign for both channels.

[5] Data and information were obtained from the IPEV/PNRA Project 'Routine Meteorological Observation at Station Concordia'; see http://www.climantartide.it.

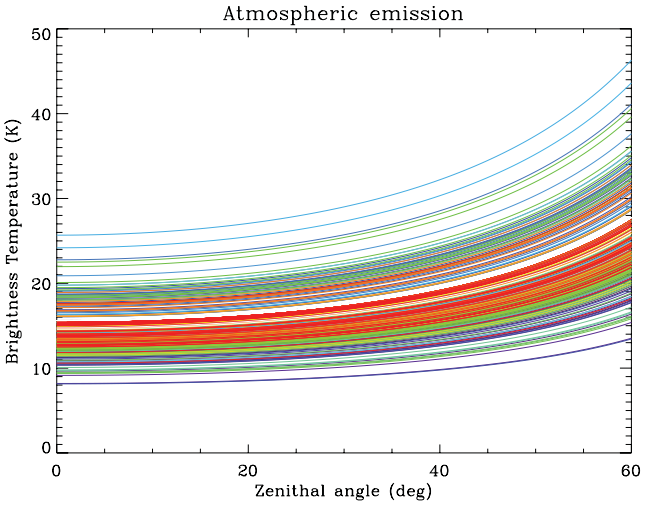

Figure 2. Collection of best-fitting curves obtained over the calibrated skydips collected during the 2009–2010 summer campaign.

5 RESULTS

5.1 Sky opacity

The distribution of the sky opacities measured during the campaign can be seen in the histogram in Fig. 3. The cyan (light) histogram is derived from channel 2 measurements while the black (dark) histogram (summed and positioned on top of the cyan histogram) is derived from channel 1 measurements. The measurements from both channels result in τ_I values centred around an average value $\langle\tau_I\rangle = 0.050$, with a median of $\tau_I^m = 0.048$ and a statistical error on each measurement of 7 per cent. This corresponds to an average transmission of 95 per cent. Although all the measurements have been taken with a clear sky, we should stress that the reported results reflect a wide variety of weather conditions and only bad weather situations (i.e. covered sky – although this is rare at Dome C) have been discarded from our analysis.

Fig. 4 shows the atmospheric transmission measurements over the whole campaign. Fig. 5 shows the same measurements averaged on

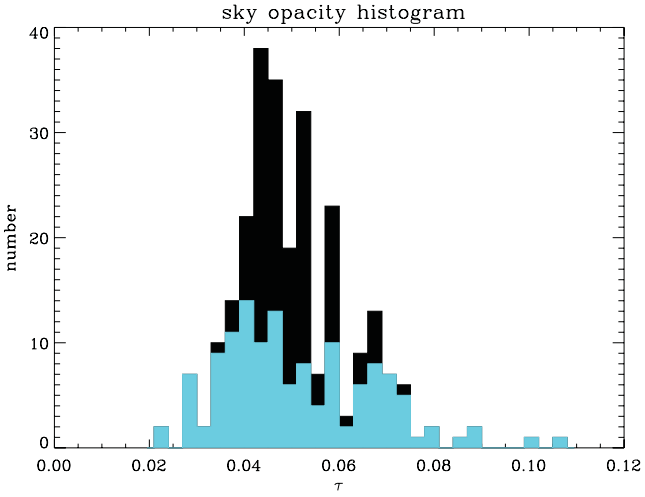

Figure 3. Histogram of measured sky opacity. The cyan (light) histogram is obtained from channel 2 measurements; the black (dark) histogram is obtained from the collection of channel 1 measurements and is positioned over the channel 2 data.

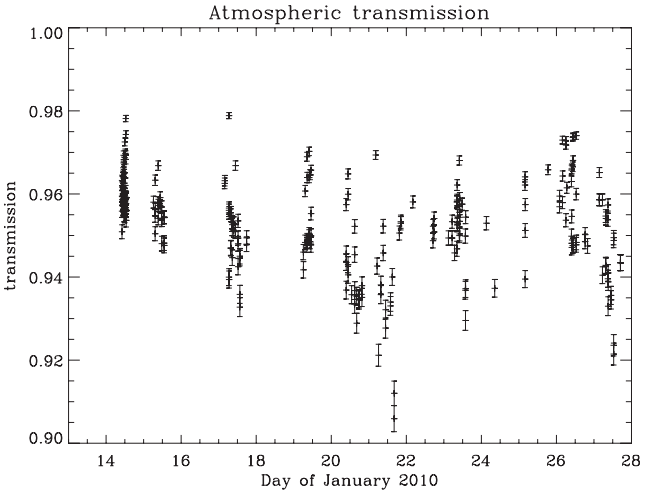

Figure 4. Atmospheric transmission during the 2009–2010 campaign. Statistical uncertainties only are shown in this graph.

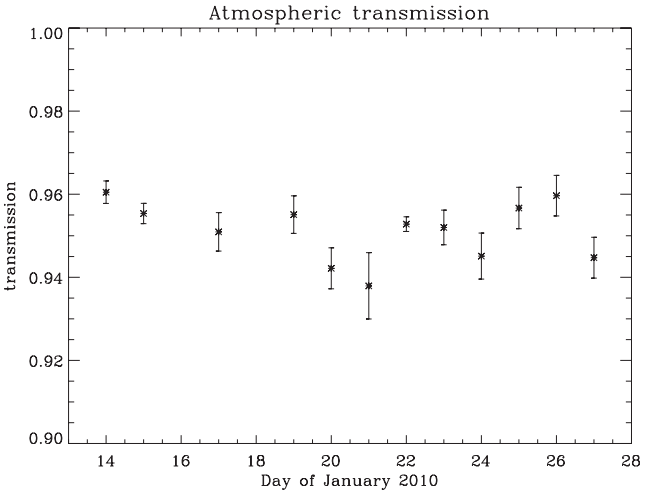

Figure 5. Atmospheric transmission during the 2009–2010 campaign. In this plot, we have averaged over the skydip acquired during the same day. This shows the general trend of the sky transmission during the campaign.

a day-by-day basis. Transmission seems to be fairly constant over the campaign, with a possible general trend to decrease in the middle of the campaign, with a rise back at the end of it. The error bars in Fig. 5 reflect the variability within each day. This parameter has to be taken into account when considering measurements with thermal detectors, such as transition edge sensor (TES) bolometers (like those planned for the QUBIC experiment), and when accounting for load variation on the bolometers themselves, and TES plus superconducting quantum interference devices (SQUIDs) working point tuning. We estimate a relative average variation, on a daily basis, of 0.9 per cent, consistent with one single tuning procedure per day needed (Battistelli et al. 2011). Peaks of a few per cent have also been observed in limited cases. This would require tuning procedures to be run more than once a day. Fig. 6 shows the transmission measured within the day. We have averaged over skydips acquired less than 2 h apart on different days. In order to reduce the scatter caused by different days of observations, we have normalized each measurement to the average daily measurements and we have multiplied by the overall average transmission. Also, in this case, the trend seems to be fairly constant, with a slight decrease

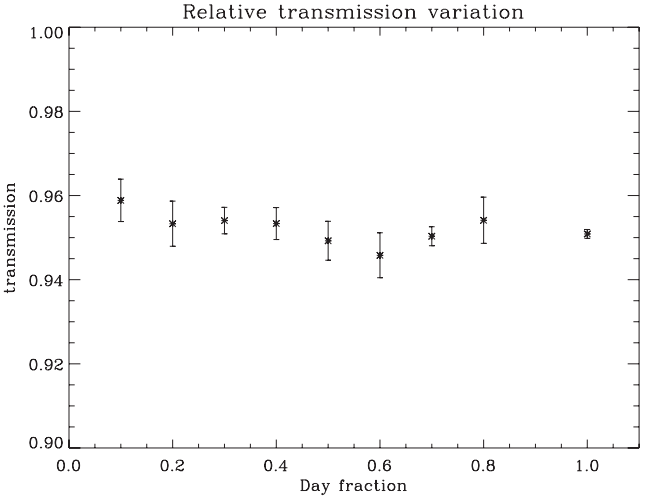

Figure 6. Atmospheric transmission during the 2009–2010 campaign. In this plot, we have averaged over the skydip acquired less than 2 h apart, each measurement being normalized by the average daily transmission, relative to (multiplied by) the overall average transmission of the campaign. This shows the general trend of the sky transmission during the day.

in the middle of the day because of the increase in elevation of the Sun.

5.2 Precipitable water vapour content

We have used the *am* model (Paine et al. 2011) to infer, from our sky opacity measurements, the characteristics – in terms of PWV – of the atmosphere over Dome C during our measurements. This model has been tailored and configured for Dome C conditions and it allows us to exploit balloon data taken during the campaign, in view of the interpretation of BRAIN data. We have found a scaling law between a photometric quantity (the brightness temperature) and an atmospheric parameter (PWV), thus removing possible degeneracies in our analysis.

Fig. 7 shows the histogram of the PWV content obtained from our skydips. These are obtained by fitting our calibrated skydips over

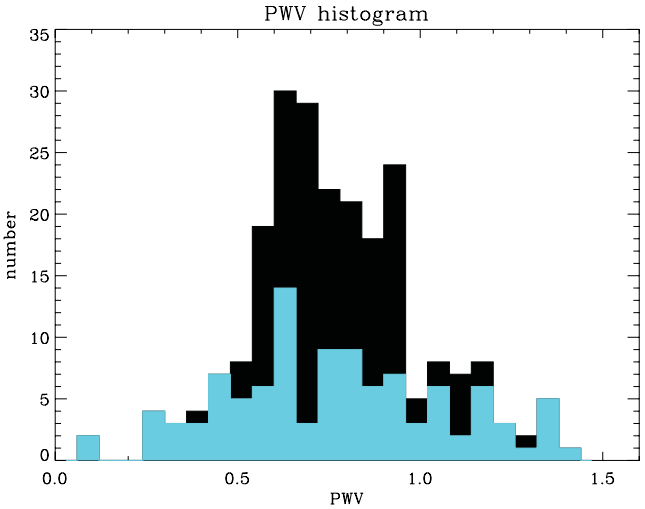

Figure 7. Histogram of the derived PWV content in the atmosphere. The cyan (light) histogram is obtained from channel 2 measurements; the black (dark) histogram is obtained from the collection of channel 1 and channel 2 measurements.

the simulated template, by only accounting for the brightness temperature change over the skydip, and not its offset, and by checking the zenith brightness temperature for consistency.

During the BRAIN-pathfinder 2009–2010 campaign we find an average PWV of $\langle PWV \rangle = 0.77$ mm, with statistical errors on each measurement of ± 0.06 mm and calibration uncertainties of $^{+0.15}_{-0.12}$ mm. We find a median of $PWV^{m} = 0.75$ mm, an average 25th percentile of $PWV^{25\text{th}} = 0.49$ mm and an average 75th percentile of $PWV^{75\text{th}} = 1.1$ mm. This level of PWV content is in good agreement with those measured in 2003–2005 and 2005–2009 with radio-sounding measurements (Tomasi et al. 2006, 2011) and with those measured by Tremblin et al. (2011) at 1.5 THz. Nevertheless, we should stress that the main results of our measurements are obtained by directly sampling the same spectral bandwidth of scientific interest and thus they are free from model-dependent bias.

5.3 Polarization

As previously mentioned, channel 2 of the BRAIN-pathfinder measures sky emission through a rotating QWP followed by a wire-grid polarizer. During observations, we rotated the QWP at several different speeds. For instrumental, environmental and noise reasons, we set its physical rotational frequency to $\nu_{\rm QWP} = 1.56$ Hz (2.09 Hz) for most of our observations. Thus, we expect any incoming circularly polarized signal to be modulated at $\nu_{\rm C} = 2 \cdot \nu_{\rm QWP} = 3.13$ Hz (4.17 Hz), and any incoming linearly polarized signal at $\nu_{\rm L} = 4\nu_{\rm QWP} = 6.26$ Hz (8.35 Hz) (see equation 1). The emission of the (ambient temperature) QWP and of the polarizer have been studied using the models presented by Salatino, de Bernardis & Masi (2011). Our data are affected by an offset modulated at both $\nu_{\rm C}$ and $\nu_{\rm L}$, which we found to be consistent with the QWP emission as well as with the polarizer emission reflected back from the QWP. We should stress that the stability of this emitted signal is critical to retrieve meaningful information from the data. One of the goals of this paper is to provide information on the polarization of the skydip signal. For the present analysis, it is critical to characterize and monitor the stability of our instrument within the average time of a skydip, because faster instability will affect the results.

We have demodulated the $\nu_{\rm C}$ and $\nu_{\rm L}$ signals using bandpass filters for each raw skydip. Thus, the extracted signals have been treated in the same way as the intensity signal in order to find a possible secant-law dependence in the polarized signal of the skydips. Once we have performed secant-law fits over the polarized skydips, we can define $\tau_{\rm C}$ and $\tau_{\rm L}$ similarly to $\tau_{\rm I}$:

$$\tau_{\rm C} = -(B^{\rm C})/(C\,T_0), \tag{6}$$

$$\tau_{\rm L} = -(B^{\rm L})/(C\,T_0). \tag{7}$$

The comparison between the different τ enables us to extract polarized information from our skydips and thus an estimation of the airmass-correlated (or anticorrelated) polarization of atmospheric emission.

Fig. 8 shows one of the skydips acquired and analysed in polarization. Polarization calibration has been performed using local polarized sources placed in the near-field and in the medium-field. However, we should stress that the derived percentage polarization levels are independent of the calibration and of the determination of the equivalent temperature of the atmosphere. The uncertainty on each of the skydip polarization levels is thus directly derived from the fits. After combining and weight-averaging over all the skydips, we find that both circular and linear polarization of the airmass-correlated signals are consistent with zero, with upper limits such that $S_{\rm C} < 0.19$ per cent and $S_{\rm L} < 0.11$ per cent (95 per cent confidence level), respectively. These results have been confirmed by cross-correlating the measured data with the signals expected from Zeeman splitting, and they are simulated using the model developed by Spinelli et al. (2011). These limits include instrumental systematics and they place a tight limit on the QWP plus polarizer stability within the time of the acquired skydips.

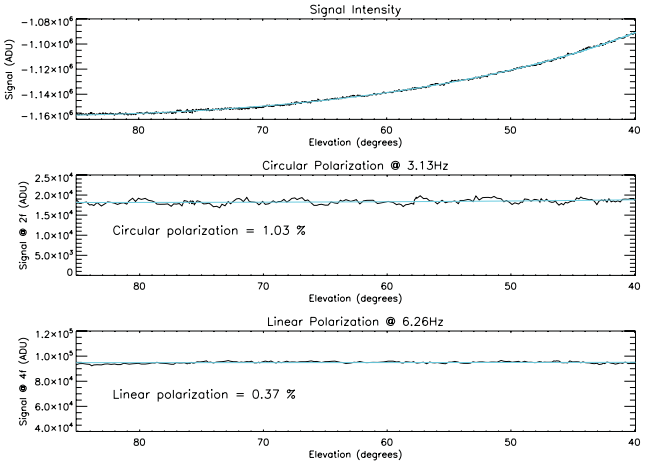

Figure 8. Intensity, linear polarization and circular polarization signal acquired during a single skydip. We plot the acquired data (dark) and the secant-law performed fit (light/cyan). We report the derivation of the percentage polarization that can be extracted from this skydip.

6 CONCLUSIONS

In this paper, we report on the detailed site testing of Dome C at 150 GHz and the first limits on the polarized emission of its atmosphere. Dome C is demonstrated to be an exceptional millimetric observational site, in terms of absolute transmission and stability, and the polarization limits are encouraging – as far as spurious polarization and intensity-polarization mixing are concerned. Our opacity measurements have been derived from a direct sampling of the frequencies of astronomical interest and thus they are free from model-dependent bias. In most observational conditions, we anticipate that the measured daily stability should enable us to have TES bolometer arrays requiring only a single tuning procedure per day. When comparing our millimetric opacities and in-bandwidth transmissions with those obtained at submillimetre wavelengths, the absolute values are one order of magnitude better in terms of transmission and stability. Nevertheless, we should keep in mind that the requirements, in terms of systematic control and stability, for a millimetric B-mode CMB experiment are such that it is necessary to characterize the atmospheric stability to a high level of precision. Our results are very encouraging. Our derived PWV value relies on a model independently developed by the BRAIN collaboration and tailored for Dome C. Our PWV values are consistent with those derived at submillimetre wavelengths (Tomasi et al. 2011). However, in our case, radiation is detected through an instrument that is similar to those that aim to detect CMB polarization, which allows direct monitoring of many systematic effects. The systematic control requirements for a B-mode CMB experiment are so stringent that no instrument, to date, has been able to meet them. The requirement for the instrumental spurious polarization induced from leakage of CMB anisotropies into B-mode polarization is that the leakage should be maintained at lower than 10^{-3} (Bock et al. 2006). This is

necessary in order to be able to reach a B-mode signal of the order of 30 nK rms (i.e. tensor-to-scalar ratio $r = 0.01$). In terms of an absolute temperature limit, our analysis does not allow us to reach this limit. However, in terms of a relative systematic limit, considering that our 0.1 per cent limit for linear polarization includes spurious polarization because of the intensity-to-polarization leakage, our instrument already satisfies this requirement.

ACKNOWLEDGMENTS

This work is supported and funded by the Progetto Nazionale Ricerche in Antartide (PNRA) and the Institut Polaire Francaise Paul Emile Victor (IPEV). We are grateful for the logistical support at Dome C. We acknowledge Dr Andrea Pellegrini for the radio sound data and information obtained from the IPEV/PNRA project 'Routine Meteorological Observation at Station Concordia – http://www.climantartide.it'. We thank Ken Ganga for comments and for reviewing the paper. We acknowledge Scott Paine (Smithsonian Astrophysical Observatory) for making the *am* code available and for kind support. We acknowledge the anonymous referee for comments that improved the paper.

REFERENCES

Archibald E. N. et al., 2002, MNRAS, 336, 1
Aristidi E. et al., 2009, A&A, 499, 955
Battistelli E. S. et al., 2008, in Duncan W. D., Holland W. S., Withington S., Zmuidzinas J., eds, Proc. SPIE Vol. 7020, Millimeter and Submillimeter Detectors and Instrumentation for Astronomy IV. SPIE, Bellingham, p. 702028
Battistelli E. et al. (QUBIC collaboration), 2011, Astropart. Phys., 34, 705
Bock J. J. et al., 2006, preprint (astro-ph/0604101)
Calisse P., Ashley M. C. B., Burton M. G., Phillips M. A., Storey J. W. V., Radford S. J. E., Peterson J. B., 2004, Publ. Astron. Soc. Australia, 21, 256
Castro P. G. et al., 2009, ApJ, 701, 857
Chiang H. C. et al., 2010, ApJ, 711, 1123
Dicke R. H., Beringer R., Kyhl R. L., Vane A. B., 1946, Phys. Rev., 70, 340
Dragovan M., Stark A. A., Pernic R., Pomerantz M. A., 1990, Appl. Opt., 29, 463
Gredel R., 2010, EAS Publ. Ser., 40, 11
Lamarre J.-M. et al., 2010, A&A, 520, A9
Lawrence J. S., Ashley M. C. B., Tokovinin A., Travouillon T., 2004, Nat, 431, 278
Masi S. et al., 2005, EAS Publ. Ser., 14, 87
Paine S., 2011, Rev. Mex. Astron. Astrofis. Ser. Conf., 41, 24
Polenta G. et al., 2007, New Astron. Rev., 51, 256
Salatino M., de Bernardis P., Masi S., 2011, A&A, 528, A138
Schillaci A., 2010, PhD thesis, Sapienza Univ. Rome
Spinelli S., Fabbian G., Tartari A., Zannoni M., Gervasi M., 2011, MNRAS, 414, 3272
Tomasi C. et al., 2006, J. Geophys. Res., 111, D20305
Tomasi C., Petkov B., Benedetti E., Valenziano L., Vitale V., 2011, J. Geophys. Res., 116, D15304
Tremblin P. et al., 2011, A&A, 535, 112
Tucker G. S. et al., 2008, in Duncan W. D., Holland W. S., Withington S., Zmuidzinas J., eds, Proc. SPIE Vol. 7020, Millimeter and Submillimeter Detectors and Instrumentation for Astronomy IV. SPIE, Bellingham, p. 70201M
Valenziano L., dall'Oglio G., 1999, Publ. Astron. Soc. Australia, 16, 167

This paper has been typeset from a TEX/LATEX file prepared by the author.